Available online at www.sciencedirect.com

Chemical Engineering Research and Design

journal homepage: www.elsevier.com/locate/cherd

Staging and path optimization of Fischer-Tropsch synthesis

Umesh Pandey, Koteswara Rao Putta, Kumar Ranjan Rout, Edd A. Blekkan, Erling Rytter, Magne Hillestad *

Department of Chemical Engineering, Norwegian University of Science and Technology, NO-7491 Trondheim, Norway

ARTICLE INFO

Article history:
Received 27 April 2022
Received in revised form 30 June 2022
Accepted 18 August 2022
Available online 5 September 2022

Keywords:
Systematic staging
Fischer-Tropsch synthesis
Path optimization

ABSTRACT

Optimization of once-through three-stage Fischer-Tropsch (FT) synthesis using path optimization is performed in this study to identify optimal structure and strategies in multi-stage FT synthesis design. The study also compares three-stage designs against recycled single-stage and two-stage designs with identical residence time and outlines key differences between different plant configurations. The results showed that it is optimal to operate at the maximum possible CO conversion and as low H_2/CO ratio as possible. The comparison of the once-through three-stage and recycled two-stage processes against recycled single-stage process showed that two-stage and three-stage processes can achieve 2.3 % and 2.7 % higher syncrude production and 2.8 % and 3.2 % higher net material value (objective function). With the possibility of recycling in all three designs, the multi-stage processes improve further: 4.2 % and 5.3 % better in terms of syncrude production and 4.2 % and 6 % better in terms of the net material value.

© 2022 The Author(s). Published by Elsevier Ltd on behalf of Institution of Chemical Engineers. This is an open access article under the CC BY license (http://creativecommons.org/licenses/by/4.0/).

1. Introduction

Fischer-Tropsch (FT) synthesis is polymerization reaction in which syngas (CO and H_2) polymerize to form n-paraffins, 1-olefins, and oxygenates. On an industrial scale, gas to liquid plants (GtL) and coal to liquid plants (CtL) utilize FT synthesis to convert syngas derived from gasification of natural gas (Carlsson, 2005) and coal to syncrude (C_{5+}) (Larson et al., 2012; Spath and Dayton, 2003), respectively. The C_{5+} is further upgraded to produce diesel/jet fuel. Similar technology has been employed in pilot/lab scale biomass to liquid (BtL) processes (Kolb et al., 2013; Hofbauer and Rauch, 2019). FT synthesis is a catalytic process that either employs shift-active catalysts like iron or less shift-active catalysts like cobalt. The FT synthesis over a cobalt catalyst is considered in this study as it offers two distinct advantages over iron-based synthesis. Firstly, the paraffin content in the C_{5+} is ca. 80–90 % (Pandey et al., 2021; Todic et al., 2014, 2015), which is important for producing high-quality jet fuel. Secondly, cobalt catalyst has higher FT activity and is more stable than the iron catalyst (Outi et al., 1981); which has been an attraction to cobalt-based synthesis in recent years.

Industrial-scale GtL or CtL plants with cobalt-based FT synthesis operate with a CO conversion of 40–60 % per pass. This is mainly to avoid loss of catalyst activity at a higher CO conversion (Jiang et al., 2020; Tucker and van Steen, 2020; Tucker et al., 2021). The loss of activity could occur either due to dilution of reactants or deactivation of cobalt catalyst in the presence of high water partial pressure (Jahangiri et al., 2014; Pandey et al., 2021). The former effect is temporary, while the latter effect is permanent and must be avoided to increase the life of the catalyst. Furthermore, high CO conversion affects the thermal characteristics of the FT reactors. The FT reactions are highly exothermic as ca. 160–165 kJ of heat is released for every mole of CO consumed (Jiang et al., 2020; Pandey et al., 2021) in the reactions. At higher CO conversion, the heat removal load becomes very high. This is

* Corresponding author.
E-mail addresses: umesh.pandey@ntnu.no (U. Pandey), magne.hillestad@ntnu.no (M. Hillestad).

https://doi.org/10.1016/j.cherd.2022.08.033

0263-8762/© 2022 The Author(s). Published by Elsevier Ltd on behalf of Institution of Chemical Engineers. This is an open access article under the CC BY license (http://creativecommons.org/licenses/by/4.0/).

Nomenclature

Acronyms

ASF	Anderson-Schulz Flory.
BtL	Biomass to liquid.
CSTR	Completely stirred tank reactor.
FT	Fischer-Tropsch.
MINLP	Mixed integer nonlinear programming.
PFR	Plug flow reactor.
WGS	Water gas shift.

Greek symbols

α	Chain growth parameter in overall polymerization reaction.
α_2	Chain growth parameter in olefin polymerization reaction.
β	Olefin-paraffin distribution parameter.
γ	Dimensionless mass flow rate relative to the inlet (W/W_0).
κ	Heat transfer area design function (kg s/m^3).
ν_i	Stoichiometric coefficient for overall polymerization reaction with i number of carbon atoms.
ν'	Stoichiometric coefficient for paraffin polymerization reaction with i number of carbon atoms.
$\nu_{[i,\infty]}$	Stoichiometric coefficient for hydrocarbon lump (C_{i+}) in overall polymerization reaction.
ν'	Stoichiometric coefficient for paraffin lump (C^p_{i+}) in paraffin polymerization reaction.
ν''	Stoichiometric coefficient for olefin lump (C^o_{i+}) in olefin polymerization reaction.
ν''	Stoichiometric coefficient for olefin polymerization reaction with i number of carbon atoms.
ω	Mass fractions of the components.
ψ	Feed distribution (kg/(m^3 s)).
σ	Residence time or space time (V_R/W_0) (m^3 s/kg).
θ	Dimensionless temperature.
ξ	Dimensionless volume of the path (V/V_R).

Roman symbols

$\bar{N}'$	Average number of carbons in the paraffin lump (C^p_{i+}).
$\bar{N}''$	Average number of carbons in the olefin lump (C^o_{i+}).
C_1–C_4	Hydrocarbons with specified number of carbons.
$C^o_2 - C^o_4$	Olefin with specified number of carbons.
C^o_{5+}	Olefin lump with 5 or more carbons.
$C^p_1 - C^p_4$	Paraffin with specified number of carbons.
C^p_{5+}	Paraffin lump with 5 or more carbons.
C_{5+}	Hydrocarbon lump with 5 or more carbons.
$\Delta_r H_j$	Enthalpy of formation of component j (kJ/mol).
E	A diagonal matrix with specific heat capacity ratio ($\frac{C_{p,ref}}{C_p}$) along the path.
K	A diagonal matrix with heat transfer design function along the path.
$\tilde{\cdot}$	Partial derivative of the component reactions (kg/(m^3 s)).
$\tilde{R}_\theta$	Rate of relative temperature increase along the path.
$\tilde{R}_i$	Formation rates of component i along the path (kg/(m^3 s)).
C_p	Specific heat capacity of gas at constant pressure (J/kg).
$C_{C_{5+}}$	Price of the syncrude ($/kg).
C_{H_2}	Price of the additional hydrogen ($/kg).
$C_{p,ref}$	Specific heat capacity of the make up gas (J/kg).
E_α	Activation energy, α-model (kJ/mol).
E_β	Activation energy, β-model (kJ/mol).
E_a	Activation energy (kJ/mol).
k	Rate constant (kmol kg$_{cat}^{-1}$ h^{-1} MPa$^{-1.5}$).
k_β	β model constant (MPa).
k_α	Growth parameter constant (MPa$^{0.265}$).
$k_{C^o_2-C^p_2}$	Ethylene hydrogenation constant.
$k_{C^p_1}$	Methanation parameter.
k_{CO_2}	WGS rate constant (kmol kg$_{cat}^{-1}$ h^{-1} MPa^{-1}).
$k_{C^o_2-olf}$	Ethylene polymerization constant.
$M_{C_{H_2}}$	Mass of the additional hydrogen (kg).
$M_{C_{5+}}$	Mass of the syncrude (kg).
p_i	Partial pressure of component i (MPa).
R_G	Universal gas constant (8.314 m^3 Pa/(k mol)).
r_i	Reaction rate for reactions defined in Eqs. (16)–(22).
T	Reactor path temperature (°C).
T_c	Coolant temperature (°C).
T_R	Reference temperature in kinetic model (483 K).
U	Stoichiometric consumption ratio of H_2/CO for overall polymerization reaction.
U'	Stoichiometric consumption ratio of H_2/CO for paraffin polymerization reaction.
U''	Stoichiometric consumption ratio of H_2/CO for olefin polymerization reaction.
U_h	Overall heat transfer coefficient (W/m^2 °C).
u_M	Mixing design function.
u_A	Active catalyst concentration design function.
u_{F1}	Recycle ratio design function.
u_F	Feed distribution design function.
u_H	Heat transfer area design function (s).
u_R	Recycle ratio.
x	Vector with mass fraction and temperature.
a	Specific heat transfer area (m^2/m^3).
y	p_{H_2O} exponent, α-model.
z	p_{CO} exponent, α-model.

not desirable as it may lead to local hot spots and potentially thermal runaway reactions.

This study primarily focuses on FT synthesis of syngas produced from gasification of biomass. The H_2/CO ratio in the syngas out of the gasifier in BtL processes are below 1.0. FT synthesis over a cobalt catalyst is typically carried at a stoichiometric H_2/CO ratio of ca. 2.05. Thus, H_2/CO ratio of the gas must be increased, preferably to ca. 2.05, either by adding external H_2 (Hillestad et al., 2018; Hannula, 2016) or utilizing WGS reaction as shown in Eq. (1) (Michailos and Bridgwater, 2019; Swanson et al., 2010; Hillestad et al., 2018).

$$CO + H_2O \underset{\text{Water gas shift reaction}}{\overset{r_{WGS}}{\rightarrow}} CO_2 + H_2 \quad (1)$$

As described here, there are design challenges associated with low per pass CO conversion and low H_2/CO ratio in

syngas feed. The overall CO conversion can be increased by introducing large recycle stream, reactor staging, or both. The staging is an interesting concept as the reactants are converted in more than one stage with separation of water and C_{5+} between the stages. The removal of water reduces temporary loss in catalyst activity due to dilution of reactants and also reduces the rate of catalyst deactivation. Hannula (2016) proposed to address the challenge with low H_2/CO ratio by adding external H_2 to the syngas feed. In their study, the addition of external H_2 increased C_{5+} production by ca 2.6 times compared to utilizing WGS reactions. This also improved the carbon efficiency of the process. The addition of external H_2 accrues significant operating costs to a BtL plants. However, recent research has shown that operating at an understoichiometric H_2/CO ratio and replenishing external H_2 between stages significantly improves production of C_{5+} and also reduces the total external H_2 requirement in the process (Rafiee and Hillestad, 2012, 2013; Hillestad et al., 2018). The staging of FT synthesis, the addition of external H_2 in the reactor feed, and the replenishment of H_2 between stages introduce an additional degree of freedom and an opportunity to employ systematic design methods and optimization techniques to identify optimal structure and strategies in FT synthesis design.

While systematic methods for process design are well established in areas like heat recovery and distillation sequencing, it is not the case for chemical reactor design. Very few methods for systematic design of reactor networks are general enough to be applicable to real non-isothermal reactor design and optimization problems. Among several methods, one of the simplest but robust reactor design method, Levenspiel (1962) plot, uses rate based reactor model to determine optimal reactor volume. Despite being a simple and intuitive method, a major drawback of this method is that it can only be used for isothermal reactions. However, it is essential to optimize other utility unit operations together with operational process parameters, coolant temperature, catalyst activity, bulk mixing, and many more for cost-effective and efficient plant operation for non-isothermal processes.

Another method for reactor design, the attainable region (AR) theory, is one of the oldest methods for improved reactor design introduced by Horn in the early 1960s, and later developed further by Glasser et al. (1987) and Feinberg (2002). In the AR theory, the reactor feed is kept constant. The product compositions is calculated for all possible reactor network configuration and represented in a geometric space. The optimum reactor configuration including the type of reactor is then found by locating the points where lines of constant objective function touches the boundary of the region. This method is easy to implement and interpret in lower dimensions, while at higher dimensions, it is almost impossible to present and interpret graphically and thus difficult to locate optimal points (Rooney et al., 2000).

Other systematic design concepts consider process intensification in optimization of reactor staging including process parameters as well as utility integration: superstructure optimization (Achenie and Biegler, 1990; Yeomans and Grossmann, 1999) and path optimization (Hillestad, 2010). Process intensification considers the possibility of integrating several unit operations instead of a conventional unit operation based optimization method. As several processes are integrated in a single unit, mass and heat transport resistance play a major role in overall process performance and optimization (Freund and Sundmacher, 2008; Peschel et al., 2010). Peschel et al. have discussed a three-level optimization concept based on process intensification, where the best reaction route and hence optimal reactor can be determined by optimization of fluxes (Peschel et al., 2010) and it is successfully implemented in optimal design of ethylene oxide reactor (Peschel et al., 2011). A more complex and rigorous optimization concept, superstructure optimization considers all possible alternative paths and employs mixed integer nonlinear programming (MINLP) for optimizing a set of integer/Boolean decision variables together with continuous design parameters. This concept has been applied for the optimization of many systems such as bio-ethanol synthesis (Martín and Grossmann, 2011), heat exchanger networks (Lotfi, 2010), and reactor networks (Achenie and Biegler, 1990).

In this paper, the path optimization concept developed by Hillestad (2010) is utilized for optimization of multi-stage FT synthesis. The path optimization structure includes the possibility to optimize reactors types (plug flow, CSTR and plug flow with back mixing), stage volume distribution, coolant temperature, feed distribution, recycling of tail gas and other design parameters for optimization of a chosen objective function (production of valuable components, investment cost, net profit, and so on). The optimization technique was successfully implemented in multistage optimization of methanol synthesis (Hillestad, 2010). The major advantage of this concept over others is that it is a simple concept which is able to include all the relevant elements of the superstructure and assist in screening of possible design which could be used as the basis framework for the detailed plant design. This study presents an optimization study of once-through three stage design and summarizes optimal design structure and strategies that can address the challenges in the FT synthesis. The design structure here refers to total reactor volume/residence time, volume distribution between stages, addition of external H_2 between stages, active catalyst concentration and recycling of the tail gas (if applicable). Further, the study presents a comparison of optimized single-stage with recycle, two-stage with recycle and three-stage FT synthesis with/out recycle.

2. Modeling Fischer-Tropsch synthesis

2.1. *The process*

A typical three-stage FT synthesis with recycle is shown in Fig. 1. The feed gas is heated to 200 °C and fed to the FT reactors. The heavy products which are liquid at reactor outlet temperature condition (> 210 °C) are knocked out after each FT stage and the gas phase is cooled down to 25 °C and three different phases are separated in a three-phase separator. Makeup H_2 is added to achieve an appropriate H_2/CO level before heating the gas to 200 °C and fed to the next stage. For a once-through process (recycle set to 0) with 60 % conversion per pass in each FT reactor, it is feasible to heat exchange between the hot product gas and cold feed gas to heat the cold gas to 200 °C.

2.2. *The synthesis gas*

A typical syngas produced from bio-gasification using pure oxygen as a gasifying agent in an entrained flow gasifier at 1300 °C (modeled in Aspen Plus) is considered as feed to the

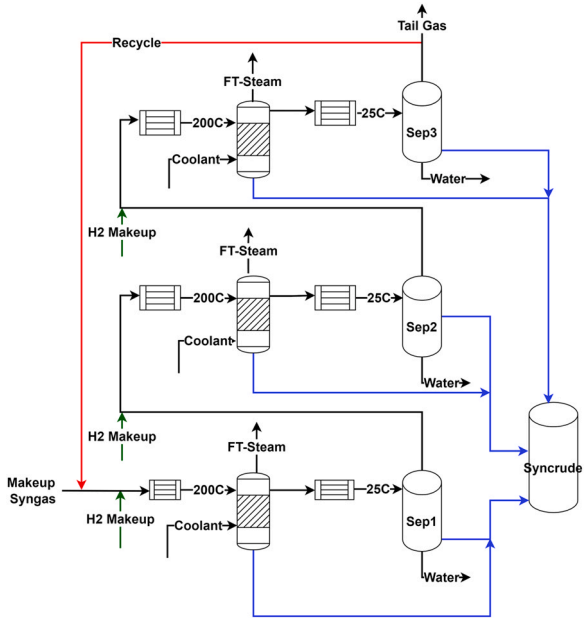

Fig. 1 – The structure of the path to be optimized. The recycle stream is set to 0 for once through process.

Table 1 – Syngas.

Temperature [°C]	200
Pressure [bar]	20.0
Molar flow [kg mol/h]	967
Mass flow [kg/h]	21,775
Mol fraction	
CO	0.5363
H_2	0.2868
H_2O	0.0030
CH_4	0.0001
CO_2	0.1233
N_2	0.0505

FT reactors. Details of the simulation can be found elsewhere (Putta et al.). Total flow rate, temperature, pressure, and compositions are shown in Table 1.

2.3. *Fischer-Tropsch reactions and kinetics*

The Fischer-Tropsch reactions are polymerization reactions in which CO and H_2 polymerize to form *n*-paraffins, 1-olefins and oxygenates. The polymerization reaction consists of an infinite number of components. Thus, the reactions and components are lumped to have a finite and describable system. Modeling of the product distribution with lumping of higher products and kinetic models of the FT reactions are discussed in detail elsewhere (Pandey et al., 2021). In the model by Pandey et al. (2021) it is assumed that the FT polymerization reaction produces olefins as primary products and paraffins as hydrogenated products. The primary product distribution is described using Anderson-Schulz Flory (ASF) distribution with chain growth probability (α) as a distribution parameter, and the olefin-paraffin distribution is described using an exponential distribution with β as a distribution parameter. Eq. (2) summarizes the primary polymerization scheme as proposed by the model. In Eq. (2), C_{5+} is a lump of C_5 and higher carbon chain products.

$$\mathrm{CO} + U(\alpha)\mathrm{H_2} \xrightarrow[\text{Overall FT polymerization}]{r} \mathrm{H_2O} + \nu_1(\alpha)\mathrm{C_1} + \nu_2(\alpha)\mathrm{C_2} + \nu_3(\alpha)\mathrm{C_3} + \nu_4(\alpha)\mathrm{C_4} + \nu_{[5,\infty]}(\alpha)\mathrm{C_{5+}} \tag{2}$$

The overall reaction is split into paraffin and olefin polymerization as shown in Eqs. (3) and (4), respectively. Here, $B = \frac{1-\alpha^2}{1-\beta^2}$.

$$\mathrm{CO} + U'\mathrm{H_2} \xrightarrow[\text{FT polymerization to paraffins}]{r_1=(1-B)r} \mathrm{H_2O} + \nu'\mathrm{C_1^p} + \nu'\mathrm{C_2^p} + \nu'\mathrm{C_3^p} + \nu'\mathrm{C_4^p} + \nu'\mathrm{C_{5+}^p} \tag{3}$$

$$\mathrm{CO} + U''\mathrm{H_2} \xrightarrow[\text{FT polymerization to olefins}]{r_2=Br} \mathrm{H_2O} + \nu''\mathrm{C_1^p} + \nu''\mathrm{C_2^o} + \nu''\mathrm{C_3^o} + \nu''\mathrm{C_4^o} + \nu''\mathrm{C_{5+}^o} \tag{4}$$

The general stoichiometric coefficients for olefins (ν'') follows ASF distribution with the distribution parameter ($\alpha_2 = \alpha\beta$). Detailed steps on formulating stoichiometric coefficients of the products (ν'') and, describing lumps could be found elsewhere (Hillestad, 2015). One can formulate ν'', lump stoichiometric coefficient (ν'') and average number of carbons ($\bar{N}''$) for olefins using Eqs. (5)–(7).

$$\nu''(\alpha_2) = (1-\alpha_2)^2\alpha_2^{i-1} \tag{5}$$

$$\nu''(\alpha_2) = (1-\alpha_2)\alpha_2^{i-1} \tag{6}$$

$$\bar{N}'' = i + \frac{\alpha_2}{1-\alpha_2} \tag{7}$$

The general stoichiometric coefficients (ν') for paraffins, average number of carbon in paraffin lumps ($\bar{N}'$), and stoichiometric coefficients for a paraffin lumps (ν') can be formulated as shown in Eqs. (8)–(10) (Pandey et al., 2021).

$$\nu' = \frac{1}{1-B}\left[(1-\alpha^2)\alpha^{i-1} - (1-\alpha)^2\alpha_2^{i-1}\right] \tag{8}$$

$$\nu' = \frac{1}{1-B}(1-\alpha)\alpha^{i-1}\left[1 - \frac{\beta^{i-1}(1-\alpha)}{1-\alpha_2}\right] \tag{9}$$

$$\bar{N}' = \left[\frac{\alpha^{i-1}(\alpha - i\alpha + i)}{(1-\alpha)^2} - \frac{\alpha_2^{i-1}(\alpha_2 - i\alpha_2 + i)}{(1-\alpha_2)^2}\right] \Big/ \left[\frac{\alpha^{i-1}}{1-\alpha} - \frac{\alpha_2^{i-1}}{1-\alpha_2}\right] \tag{10}$$

The stoichiometric hydrogen utilization ratio, U' for paraffins and U'' for olefins can be formulated as shown in Eqs. (11) and (12), respectively (Pandey et al., 2021).

$$U' = 2 + \frac{1-\alpha}{1-\beta}\left(1 - \frac{1-\alpha}{1-\alpha_2}\right) \tag{11}$$

$$U'' = 2 + (1-\alpha_2)^2 \tag{12}$$

In addition to the Eqs. (3) and (4), four additional reactions, Eqs. (13)–(15) and (1), were considered to address the anomalies which could not be described by combination of ASF and paraffin-olefin distribution (Pandey et al., 2021). Here, ethylene polymerization reaction (14) is formulated similar to the olefins polymerization; therefore, Eqs. (5)–(7) with a distribution parameter (α_2) could be used to describe the product distribution.

Table 2 – Kinetic Parameters of postulated reaction kinetics (Pandey et al., 2021).

Rate constant (k) [kmol kg_{cat}^{-1} h^{-1} $MPa^{-1.5}$]	10.85
Activation energy (E_a) [kJ/mol]	92.0
Adsorption coefficients	
a'[MPa^{-1}]	12.0
b[$MPa^{-0.5}$]	1.10
f[MPa^{-1}]	1.25
Methanation constant ($k_{C_1^p}$) [–]	6.38
Ethylene polymerization constant ($k_{C_2^o\text{-olf}}$) [–]	0.67
Ethylene hydrogenation constant ($k_{C_2^o-C_2^p}$) [–]	0.27
WGS rate constant (k_{CO_2})[kmol kg_{cat}^{-1} h^{-1} MPa^{-1}]	119.1
Growth parameter constant (k_α) [$MPa^{0.265}$]	0.095
Activation energy, α-model, (E_α) [kJ/mol]	4.77
p_{CO} Exponent, α-model (z) [–]	0.17
p_{H_2O} Exponent, α-model (y) [–]	0.095
β model constant (k_β) [MPa]	0.16
Activation energy, β-model, (E_β) [kJ/mol]	42.7

$$CO + 3H_2 \xrightarrow[\text{Methanation reaction}]{r_3} C_1^p + H_2O \tag{13}$$

$$(1-\alpha_2)C_2^o + CO + 2H_2 \xrightarrow[\text{Ethylene polymerization}]{r_4} \nu'''(\alpha_2)C_3^o + \nu'''(\alpha_2)C_4^o + \nu_{[5,\infty]}(\alpha_2)C_{5+}^o + H_2O \tag{14}$$

$$C_2^o + H_2 \xrightarrow[\text{Ethylene Hydrogenation}]{r_5} C_2^p \tag{15}$$

The rate of formation of FT products (r_{FT}) and other kinetic rates r_1–r_6 are described using Eqs. (16)–(22) (Pandey et al., 2021). The product distribution parameters (α and β) are described using Eqs. (23) and (24). The α model, Eq. (23), suggests that higher water partial pressure, lower H_2/CO ratio favors and lower temperature favors higher products while r_{FT} is mostly dependent on the reactant partial pressures. The kinetic parameters here are as reported by Pandey et al. (2021) with parameters k_a, k_α and k_β has been modified using the lab synthesis data for the catalyst considered in this study. The values of kinetic parameters used in Eqs. (16)–(24) are summarized in Table 2. In Eq. (19), $r_{C_1^p,\text{ideal}} = \nu' r_1 + \nu'' r_2$, and in Eqs. (20) and (21), $r_{C_2^o,\text{ideal}} = \nu'' r_2$.

$$\text{Primary reaction}: r_{FT} = \frac{k e^{-\frac{E_a}{R_G}\left(\frac{1}{T}-\frac{1}{T_R}\right)} \cdot p_{CO} p_{H_2}^{1/2} (1 + 0.1 p_{H_2O})}{(1 + a' p_{CO} + b p_{H_2}^{1/2} + f' p_{H_2O})^2} \tag{16}$$

$$\text{Paraffin reaction}: r_1 = (1-B) r \tag{17}$$

$$\text{Olefin reaction}: r_2 = B r \tag{18}$$

$$\text{Methanation reaction}: r_3 = k_{C_1^p} \cdot r_{C_1^p,\text{ideal}} \cdot p_{H_2} \tag{19}$$

$$\text{Ethylene polymerization reaction}: r_4 = k_{C_2^o-\text{olf}} \cdot \frac{r_{C_2^o,\text{ideal}}}{1-\alpha_2} \tag{20}$$

$$\text{Ethylene hydrogenation reaction}: r_5 = k_{C_2^o-C_2^p} \cdot r_{C_2^o,\text{ideal}} \tag{21}$$

$$\text{WGS reaction}: r_6 = k_{CO_2} e^{-\frac{47400}{R_G T}} \left(p_{CO} p_{H_2O} - p_{CO_2} p_{H_2}\right) \tag{22}$$

$$\text{Growth parameter}: \alpha = \frac{1}{1 + k_\alpha e^{-\frac{E_\alpha}{R_G}\left(\frac{1}{T}-\frac{1}{T_R}\right)} / p_{CO}^z p_{H_2O}^y} \tag{23}$$

$$\text{Olefin-Paraffin distribution parameter}: \beta = \frac{1}{1 + \frac{k_\beta e^{-\frac{E_\beta}{R_G}\left(\frac{1}{T}-\frac{1}{T_R}\right)}}{p_{CO}}} \tag{24}$$

2.4. Fischer-Tropsch reactors and catalysts

Four different reactor technologies, slurry bed reactors, fluidized bed reactors, fixed bed reactors and microchannel reactors, are suitable for Fischer-Tropsch synthesis, and had been developed and employed in industrial applications (Evans and Smith, 2012). This paper aims to propose design alternatives with the staging of fixed bed reactors as it is one of the most matured technologies available. The temperature in the catalytic fixed bed reactors can easily be controlled by adjusting the boiling pressure of the cooling liquid (water in this study) in the reactor shell. This is very advantageous for catalytic processes such as FT synthesis as one can easily compensate for the loss of catalyst activity by adjusting the boiling pressure.

One of the critical design challenges in FT synthesis arises from its exothermic reactions (160–165 kJ for 1 mol of CO consumption (Saeidi et al., 2014)), possibly leading to thermal runaway reactions. Heat transfer is one of the key parts of the FTS design and is even more critical for the fixed bed reactors (usually modeled as plug flow reactors (PFRs)) due to their tendency to form local hot-spots. To avoid runaway reactions and minimize local hot-spots, 1 in. reactor tubes with 10 m bed length are considered for the stage optimization. The tube dimensions are in the range as recommended in patents (Espinoza et al., 2006; Hardeveld et al., 2013). The idea here is to choose reactor tubes with as small diameter as feasible to increase the specific heat transfer area $a = 4/d_t$ and increase the heat transfer rate of the FT reactors. The catalyst considered here is a LTFT catalyst, 20%Co/0.5Reγ–Al_2O_3, with a maximum allowable catalyst concentration of 200 kg/m^3, typically arranged as an eggshell structure with active catalyst phase impregnated on the alumina pellets.

3. Path optimization

The path optimization method, described in the paper by Hillestad (2010), is applied here. A path is a line of production and represents the process from starting material to final or intermediate products. Phenomena like reaction, heat transfer, phase separation and mixing may take place on the path. A concise model that describes the rate at which the phenomena take place, must be available. Most importantly, a model describing the reaction kinetics and product distribution are necessary. The method is explained in detail in the paper by Hillestad (2010). Extensions of the method is implemented here, where the method is used for screening of the FT reactor systems (from syngas to the products) consisting of one, two and three different stages together with product separation between stages.

The reactor path is divided into any number of stages and the design functions are optimized in order to maximize an objective function. The design functions considered in this study are summarized in Table 3. The flow model, Eqs. (25) and (26), represents the change of state variables along the path (Hillestad, 2010):

Table 3 – Optimization variables.

Description	Symbol	Upper bound	lower bound
FT volume distribution	$\frac{\Delta V}{V}$	0	1
Hydrogen feed distribution	u_F	0.0	0.1
FT coolant temperatures	T_c	210 °C	225 °C
Catalyst activity/dilution	u_A	0.0	1.0
Space time (V_R/W_0)	σ	0 m^3 s/kg	100 m^3 s/kg

$$[\gamma, -u_M\sigma\tilde{-}]\frac{d[}{d\xi} = \sigma u_A\bar{5}([) + u_F.([_F - [) + u_{F1}.([_{F1} - [) - u_H((([- [_w) \quad (25)$$

$$\frac{d\gamma}{d\xi} = u_F - u_S + u_{F1} \quad (26)$$

Here, γ is the dimensionless mass flow rate relative to the inlet (W/W_0), u_M is the mixing design function, and σ is residence time or space time defined as $\sigma = V_R/W_0$. Furthermore, $\tilde{-}$ is the partial derivative of component reactions with respect to the state vector **x**, which is defined as shown in Eq. (27).

$$\tilde{-} = \frac{\partial\bar{5}([)}{\partial[} + \mathrm{diag}(0, \ldots 0, 1)\left[\psi\left(1 - \frac{C_{p,F}}{C_p}\right) - \kappa\frac{C_{p,ref}}{C_{p,0}}\right] \quad (27)$$

The feed distribution is ψ in kg/(m^3 s), κ is the heat transfer area design function, $\kappa = \frac{U_a}{C_{p,ref}}$ in kg/(m^3 s) ξ is the dimensionless volume of the path (V/V_R). u_A is the active catalyst concentration function. u_F is the feed distribution design function, $u_F = \sigma\psi$. u_{F1} is the feed distribution design function, $u_{F1} = u_R\frac{\gamma(1-u_S)}{W_0}$. u_R is the recycle fraction of the tail gas. **K** is a diagonal matrix, $. = \mathrm{diag}(1, 1, \ldots, \frac{C_{p,F}}{C_p})$. u_H is the heat transfer area distribution function, $u_H = \sigma\kappa$. **E** is a diagonal matrix, $(= \mathrm{diag}(0, 0, \ldots, \frac{C_{p,ref}}{C_p})$. [**x**] is the vector of mass fractions augmented with dimensionless temperature.

$$[= [\omega_{CO}, \omega_{H_2}, \omega_{H_2O}, \omega_{N_2}, \omega_{C_1}, \omega_{C_2^p}, \omega_{C_3^p}, \omega_{C_4^p}, \omega_{C_2^o}, \omega_{C_3^o}, \omega_{C_4^o}, \omega_{C_{5+}}, \theta] \quad (28)$$

Here, ω_i is mass fraction of the component i and $\omega_{C_{5+}} = \omega_{C_{5+}^p} + \omega_{C_{5+}^o}$. θ is the dimensionless temperature, $\theta = (T - T_{ref})/T_{ref}$.

$\bar{5}([)$ is the reaction rate vector on a mass basis, kg/(m^3 s)

$$\bar{5}([) = [\tilde{R}_{CO}, \tilde{R}_{H_2}, \tilde{R}_{H_2O}, \tilde{R}_{N_2}, \tilde{R}_{C_1}, \tilde{R}_{C_2^p}, \tilde{R}_{C_3^p}, \tilde{R}_{C_4^p}, \tilde{R}_{C_2^o}, \tilde{R}_{C_3^o}, \tilde{R}_{C_4^o}, \tilde{R}_{C_{5+}}, \tilde{R}_\theta]^T \quad (29)$$

here, $\tilde{R}_{C_{5+}} = \tilde{R}_{C_{5+}^p} + \tilde{R}_{C_{5+}^o}$ and $\tilde{R}_{C_1} = \tilde{R}_{C_1^p} + \tilde{R}_{C_1^o}$. $\tilde{R}_\theta$ is defined as:

$$\tilde{R}_\theta = \frac{\sum(-\Delta_r H_j)r_j}{C_p T_{ref}} \quad (30)$$

Explanation of the terms in Eq. (25) are as follows: the first term on the right is mass consumption or production due to reactions, the second term accounts for extra feed stream, the third term accounts for recycling of tail gas, and the last terms accounts for the heat added or removed from the reactor path. A brief explanation of the different design functions is given here and more details can be obtained in Hillestad (2010).

Mixing: This design function is denoted by u_M and it can have values between zero and one. When it is zero, Eq. (25) represents a plug flow model with completely segregated flow and when it is one, it represents a completely mixed flow or CSTRs. For values between zero and one, the mixing structure will be a plug flow with internal recycling. In this study, u_M is set to 0 meaning PFRs are considered here for the optimized design. When optimization is performed for maximization of C_{5+}^p including mixing structure in the optimization, a completely mixed reactor (CSTR) is a preferred option. However, the difference in optimal values is very small between completely mixed (CSTR) reactor and segregated flow (PFR) reactors.

Heat transfer: The design function $u_H = U_h a\mathcal{C}_{p,ref}$ defines the heat transfer area distribution along the path. The function is dimensionless, where U_h is the overall heat transfer coefficient and a is the specific heat transfer area in m^2/m^3.

Distributed feed: The design function $u_F = \psi\sigma$ represents the distribution of additional feed along the path. Here, only the addition of extra hydrogen feed at the reactor inlet ($\zeta = 0$) is considered for the sake of simplicity in process design.

Chemical reactions: The design function u_A is the relative catalyst activity or catalyst dilution and it can vary between zero and one.

The optimal reactor configuration can be found by solving the following optimization problem:

$$\max_{[\sigma,\mathbf{X}]\in\mathscr{U}} J \quad (31)$$

$$\text{s. t. } \frac{d]}{d\xi} = \mathbf{I}(], \mathbf{X}); \quad](0) =]_0 \quad (32)$$

$$\mathbf{K}(], u) \leqslant \quad (33)$$

where: $] = [[^T, \gamma]^T$ and $\mathscr{U}$ is the design space and J is the objective function. The model equations are discretized by the orthogonal collocation method and formulated as nonlinear equality constraints and the optimization problem is solved through infeasible path optimization, i.e., both model variables and design variables are iteratively optimized such that the final solution satisfies both model constraints (equality constraints) and design constraints (equality and inequality constraints). Path constraints on the state variables are represented by nonlinear inequality constraints.

3.1. Optimization variables

The optimization variables are summarized in Table 3. Total reactor volume of the FT synthesis (space-time) as well as the volume distribution between stages, hydrogen distribution, reactor coolant temperatures, and catalyst dilution are subject to optimization. Furthermore, the catalyst activity or catalyst dilution at each stage may change. The activity is a number between 0 and 1 relative to the kinetics, 1 being the undiluted catalyst describing the intrinsic kinetics. The specific area of heat transfer in FT reactors could be considered for optimization, however, in this paper, the heat transfer design variable u_H is fixed as reactor tubes with 1 in. diameter are selected upfront for the FT synthesis. Thus, $\kappa = U_h a/C_{p,ref} = constant$, where $a = 4/d_t = 160\ m^2/m^3$ and overall heat transfer coefficient is assumed to be 400 W/m^2 K. For the sake of simplicity of the FT synthesis, a single coolant liquid temperature between 200 and 225 °C is optimized for all three stages of a once through three-stage design. This simplification reduces the need for extra units of a steam drum and boiler water feed due to increase in the number of stage from 1 to 3 in once through three-stage design.

3.2. Optimization constraints

The maximum allowed reactor temperature along the path is set to 225 °C. The reason is that the catalyst life is prolonged

Table 4 – Optimized design variables (volume distribution, catalyst concentration, coolant temperature, makeup H_2 requirement) and production characteristics (net annualized material revenue, C_{5+} production, CO conversion and carbon efficiency) for once-through three-stage process.

Stage	Mass flow $\frac{W}{W_0}$ [–]	Space time $\frac{V}{W_0}$ [m^3 s/kg]	C_{5+} production $\frac{W_{H_2}}{W_0}$ [–]	Makeup H2 $\frac{W_{C_{5+}}}{W_0}$ [–]	CO conversion X_{CO} [%]	C_{5+} selectivity $\frac{W_{C,C_{5+}}}{W_{C,0}}$ [%]	Catalyst Conc^n [kg/m^3]	Coolant temperature [°C]
First	1.065	3.47 (64.4 %)	0.174 (64.4 %)	0.055 (75.1 %)	60	85.7	200	
Second	0.645	1.35 (25.0 %)	0.068 (25.2 %)	0.013 (17.6 %)	60	85.3	200	210.9
Third	0.480	0.57 (10.6 %)	0.028 (10.4 %)	0.005 (7.3 %)	60	84.4	200	
Total	–	5.39	0.270	0.073	93.6	85.4		

when the temperature is kept low and it is possible to avoid runaway reactions at a moderate temperature for the FTS reactions. Catalyst deactivation increases exponentially with temperature. Therefore, temperatures along the reactors are controlled by inequality constraints. In addition, CO conversion plays a key role in the catalyst deactivation (Pandey et al., 2021) and increases with higher conversion due to prevalence of water-induced deactivation (Gavrilović et al., 2021; Stors, 2005; Dalai and Davis, 2008). Thus per pass maximum conversion is fixed to 60 %. The inlet temperature of all the stages is set to 200 °C. In addition, there is a cooler taking the temperature down to ca 25 °C for the heavy hydrocarbon products and water to be condensed to liquid and separated. In addition to the temperature constraints, other constraints include model constraints which are well described in Hillestad (2010).

3.3. Objective function

As explained by Hillestad (2010), objective functions can be defined as maximization of heavy hydrocarbon production, total conversion, energy efficiency and return on investment (ROI), to name a few. An annualized revenue function (yearly operating hour = 8000 h) is formulated for optimization of three-stage FT synthesis. The objective function here is to maximize the net economic output of the products including makeup hydrogen cost and annualized fixed bed reactor costs for once through three-stage FT synthesis. The total annualized cost of 1 m^3 LTFT reactors was estimated to be M$ 0.265 using economic data from Swanson et al. (2010). The idea of including reactor cost is to size the required bed volume for the optimal objective function. The syncrude (density of 624 kg/m^3) price ($C_{C_{5+}}$) is taken as $297/bbl or $3 /kg and renewable makeup H_2 cost is taken as $3/kg which is a typical cost as mentioned by the Hydrogen council (2020). The syncrude price considered here corresponds to a levelized price estimated by preliminary techno-economic analysis of a conventional BtL plantX. The estimated levelized syncrude price $C_{C_{5+}}$ is significantly higher than the conventional crude oil price and the objective function J is highly sensitive to $C_{C_{5+}}$. However, the higher value is chosen as it represents a typical levelized cost for a small scale conventional BtL Plants that are exempt from CO_2 taxes. The characteristics of the optimized results in terms of stage volume distribution, recycle ratio, feed distribution, cooling temperature characteristics, active catalyst concentration are insensitive to the changes in $C_{C_{5+}}$.

$$J = C_{C_{5+}} M_{C_{5+}} - C_{H_2} M_{H_2} - C_R \tag{34}$$

$$C_R = 0.265 \cdot 10^6 \cdot V_R^{0.6} \tag{35}$$

Here, V_R is the total reactor volume in m^3. The technique is further extended to compare single-stage, two-stage and three-stage FT synthesis design. For this comparison, an objective function with net annual material revenue (annual operating hour = 8000 h) is considered for the optimization.

$$J = C_{C_{5+}} M_{C_{5+}} - C_{H_2} M_{H_2} \tag{36}$$

3.4. Optimization numeric

The optimization problem was implemented in MATLAB. The optimization problem is a nonlinear programming as it includes complex FT kinetic model. This requires much more sophisticated optimization solver than a local optimization solver like *fmincon* to find a global optima. In this study, *MultiStart* global optimization solver was used to find the global optima of the problem. *MultiStart* generates trial start points using a scatter-search mechanism (or user provides trial points) and then implements a local optimization solver (Ugray et al., 2007) at each trial points. In this case, *active-set* algorithm based *fmincon* solver was used to find local solution with different trial start points. Even though the solution from the *MultiStart* might not be exactly a global solution, the solution is assumed to be a global solution.

4. Results and discussions

4.1. Once through three-stage synthesis

The path optimization was performed for once-through three-stage FT synthesis ($u_{F1} = 0$) and the revenue function in Eq. (34) was optimized. The annualized revenue function (J) for the optimized once-through three-stage design is M$ 15.61 per kg/s of syngas feed (M$ 101 per year for syngas feed in Table 1). The results of the optimization are listed in Table 4. For a typical optimized once through three-stage FT synthesis, the optimal space-time is 5.39 m^3 s/kg which amounts to 6642 tubes for the syngas flow in Table 1. The tubes are distributed as 64.4 % (4277 tubes), 25.0 % (1660 tubes) and 10.6 % (704 tubes) for the first stage, second stage and final stage respectively. The distribution is proportional to overall material flows and total C_{5+} production. In the optimal scenario with proposed design configuration, the production of syn-crude (C_{5+}) is 0.27 kg per kg/s of syngas (or 5880 kg/h for syngas in Table 1) with 64.4 %, and 25.2 % of production coming from the first two-stages. The optimal coolant temperature is 210.9 °C. The optimal H2 requirement to maintain this production is 0.073 kg of H_2 per kg of syngas with 75.1 % fed to the first stage and 17.6 % fed to the second stage. The overall CO conversion is 93.6 % with 60 % per pass conversion for all the stages indicating that the constraints on the conversion is the

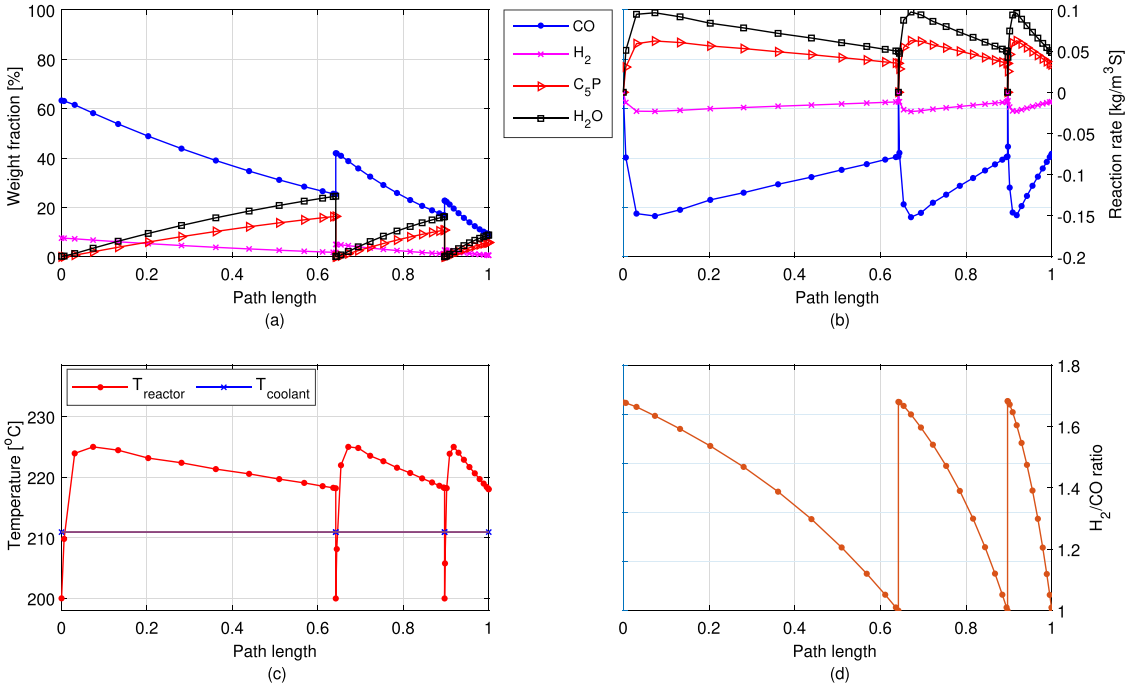

Fig. 2 – (a) Mass concentration, (b) temperature, (c) reaction rate and H_2/CO profile for once-through three-stage optimized design.

bottleneck in the optimal design and the results could be different for different catalyst characteristics with higher resistance to deactivation due to higher water partial pressure.

The profiles for the optimized design are shown in Fig. 2. The figure shows the weight fraction of the key components, reaction rates, temperature profile and H_2/CO profiles plotted against path length, where the path is proportional to the volume distribution of the reactors in each stage. The switching between stages is indicated here by-product separation and feed gas heated to 200 °C which then react to give reaction rates as shown in the same figure. The results shows the reactor feed is under-stoichiometric (H_2/CO is 1.67) for each stages and outlet syngas H_2/CO is 1.0. The optimization results suggest that it is beneficial to have as low H_2/CO as possible which can be traced back to the kinetics of the cobalt catalyst and the structure of the objective function. The objective function J has three terms where revenue term ($C_{C_{5+}} M_{C_{5+}}$) and H_2 cost term ($C_{H_2} M_{H_2}$) are the most significant. Thus, maximizing the objective function tends to maximize the production and minimize makeup H_2 feeding. For this reason, the optimal solution converges at as low H_2/CO as possible. In addition, the production of C_{5+} is dependent on the conversion and selectivity to C_{5+}. With the limit on maximum possible per pass conversion due to catalyst characteristics, an ideal optimization strategy is to increase the selectivity to C_{5+} thereby maximizing the production of valuable products which ultimately maximizes the objective function J. The kinetic characteristics suggest that lower reactor bed temperature, and lower H_2/CO ratio increases the selectivity to C_{5+} as highlighted by Pandey et al. (2021) showing added benefit of operating at as low H_2/CO as possible. However, lowering of the H_2/CO below 1.0 is not favorable as the catalyst deactivates much faster at H_2/CO < 1.0 (Gavrilović et al., 2021; Pandey et al., 2021).

The reactor operating temperature has two contrasting effects on the objective function. In general, coolant temperature controls the temperature in the bed which affects the reaction kinetics (total conversion) and product selectivities. The reaction rate increases significantly with the temperature and, for the FT synthesis over a cobalt catalyst, the rate increases mildly

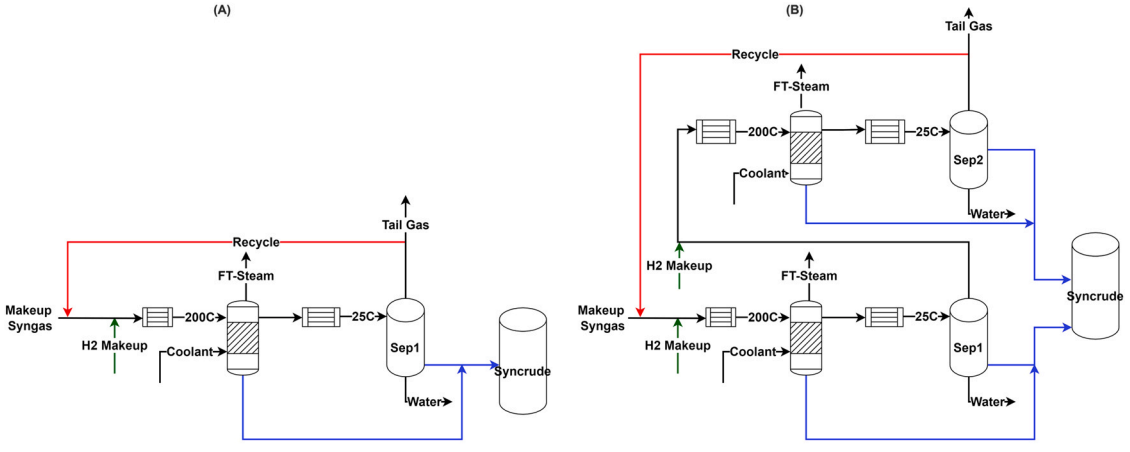

Fig. 3 – An FT synthesis superstructure of single-stage process (A) and two-stage process (B) with recycle of tail gas.

Table 5 – Optimized design variables (recycle ratio, volume distribution, catalyst concentration, coolant temperature, makeup H_2 requirement) and production characteristics (net annualized material revenue, C_{5+} production, CO conversion and carbon efficiency) for the single-stage, two-stage and three-stage design. The maximum total conversion is constrained to 93.6 %. The optimized CO-conversion per stage for all cases is 60 % and the space time (σ) is set to 5.39 m^3 per kg/s of syngas feed.

Number of stages	Net annualized material revenue [M$/year] per kg/s syngas	Recycle ratio $\frac{W_R}{W_0}$ [–]	Volume distribution $\frac{V_{stage}}{V}$ [%]	Makeup H_2 [–]	C_{5+} production $\frac{W_{C_{5+}}}{W_0}$ [–]	CO conversion X_{CO} [%]	Carbon efficiency $\frac{W_{C,C_{5+}}}{W_{C,0}}$ [%]	Catalyst Conc^n[Kg/m^3]	Coolant T [°C]
1	16.47	2.66	–	0.072	0.263	91.8	77.8	200	210.2
2	16.93	0.72	71.4 % & 28.4 %	0.073	0.269	93.6	79.6	200	210.5
3	16.99	0.00	64.4 %, 25.0 % & 10.6 %	0.073	0.270	93.6	79.9	200	210.9

with the H_2/CO ratio. Lower operating temperature while operating at the under-stoichiometric H_2/CO requires a very large reactor volume to maintain the per pass conversion of 60 % and ultimately reduces the objective function J due to an increase in the reactor cost term (C_R) in J. On the other hand, lower coolant temperature has some positive effect as selectivity to C_{5+} is higher at lower temperature and thus has a small positive effect on the objective function J. However, the effect of loss in conversion due to lower coolant temperature or requirement of large reactor volume to obtain similar conversion has a much higher negative impact on the objective function J than the small positive effect due to the slight increase in the C_{5+} selectivity. Hence, the results suggest operating at 210.9 °C which is able to maintain a stable operating condition as shown in Fig. 2, avoiding thermal runaway reaction (the peak temperature is the same as the maximum allowable temperature) and still maintaining the stable production with a maximum allowable per pass conversion. In the case of catalyst concentration, the solution is to operate at as a high concentration as possible to maintain the reaction rates and the total CO conversion. The results here are very much dependent on the kinetics which in turn depends on the catalyst characteristics. For a different type of catalyst, the constraint might be different but one can follow the steps highlighted in this study and obtain the optimal solution which could be then implemented in a detailed BtL plant design.

4.2. *Comparison of three-stage design against single-stage and two-stage design*

The technique is then used to compare optimized design for a single-stage, two-stage and three-stage synthesis. The single-stage and two-stage processes considered here are shown in Fig. 3. In this case, a recycle stream from the last stage of tail gas is introduced and a comparison of single-stage with two-stage and three-stage operation is performed by introducing the following criteria: .

- Maximum N_2 mole fraction of 0.1 (feed molar N_2 fraction is 5.05 %) at the feed inlet of the first stage of the reactor.
- Two different comparison studies are performed with constraints on the total conversion and no constraints on the total possible conversion. In the first case, a maximum possible conversion after recycling was set to 93.6 % which corresponds to the total conversion of the once-through process as optimized in the prior section. This enables comparison of three-stage once-through process with recycled single and two-stage operation. In the second comparison, the maximum possible conversion is set to 100 %.
- The space-time or bed volume to makeup gas flow ratio is set to 5.39 m^3 per kg/s of the feed. The space-time here corresponds to an optimized once-through three-stage FT synthesis design.
- The makeup gas flow is constant and the optimization model is allowed to suggest best possible makeup H_2 integration for single-stage, two-stage and three-stage design.
- Note that the recycle is internal in the FT section, i.e., there is no recycle back to syngas generation.

4.2.1. *Comparison of once through three-stage design against recycled single-stage and two-stage design*

The results for comparison between a single-stage, two-stage and three-stage design with a maximum possible conversion of 93.6 % are summarized in Table 5. The two-stage and three-

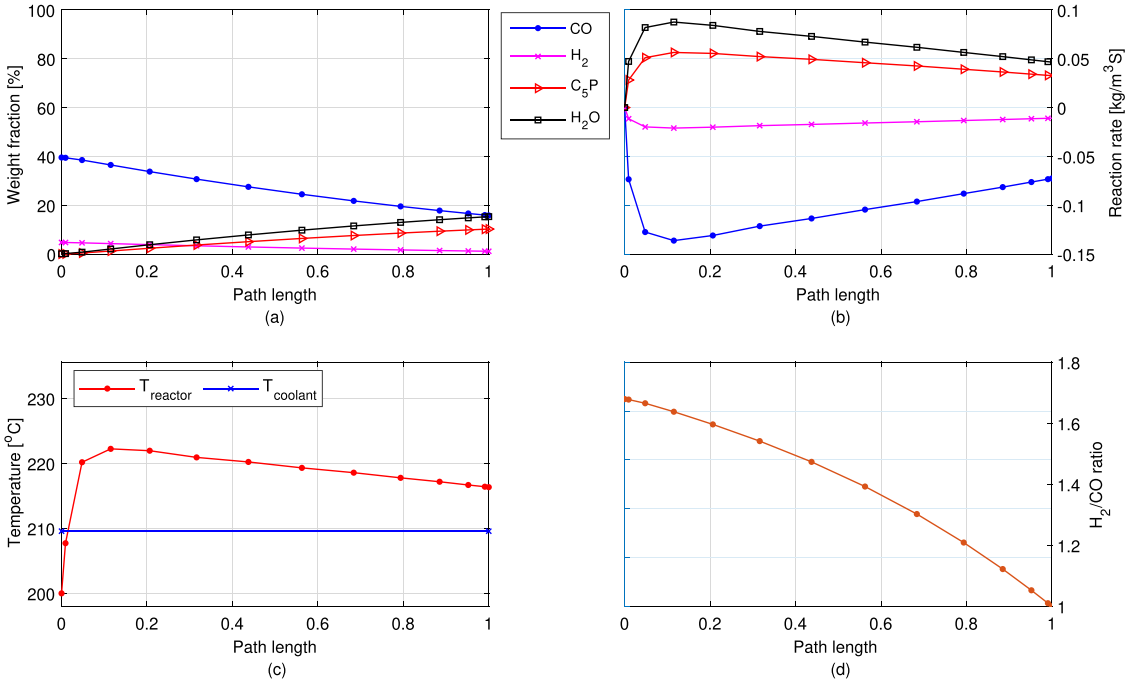

Fig. 4 – (a) Mass concentration, (b) temperature, (c) reaction rate and (d) H_2/CO profile for single-stage optimized design. The space time (σ) is set to 5.39 m^3 per kg/s of syngas feed.

stage are 2.8 % and 3.2 % better in terms of net material value and 2.3 % and 2.7 % better in terms of C_{5+} production in comparison to the optimized single-stage design. The total conversion is 91.8 % and 93.6 % for single-stage and two-stage optimized designs while CO conversion is still 60 % for each stage in single-stage, two-stage and three-stage designs. The overall improvement in the carbon efficiency is comparable (1.8 % and 2.1 % higher), however, the comparable performance comes at the cost of a huge recycle to makeup gas ratio of 2.66 in comparison to 0.72 for the two-stage design and no recycle for the once-through three-stage design. The results for the optimal design for two-stage and three-stage are very similar with less than 1 % overall improvement in net economic output, total conversion and C_{5+} production at the cost of additional stages for the three-stage design and active cost of additional recycle compressor for the two-stage design. The choice between these two options comes down to the design criterion of selection over active cost unit in terms of recycle compressor and passive cost unit in terms of additional separator and heat exchanger units.

The mass concentration, reaction rate, H_2/CO profile and temperature profile for the single-stage and two-stage optimal design with recycling of the tail gas is shown in Figs. 4 and 5. The mass fraction profile (Fig. 4) shows that the weight

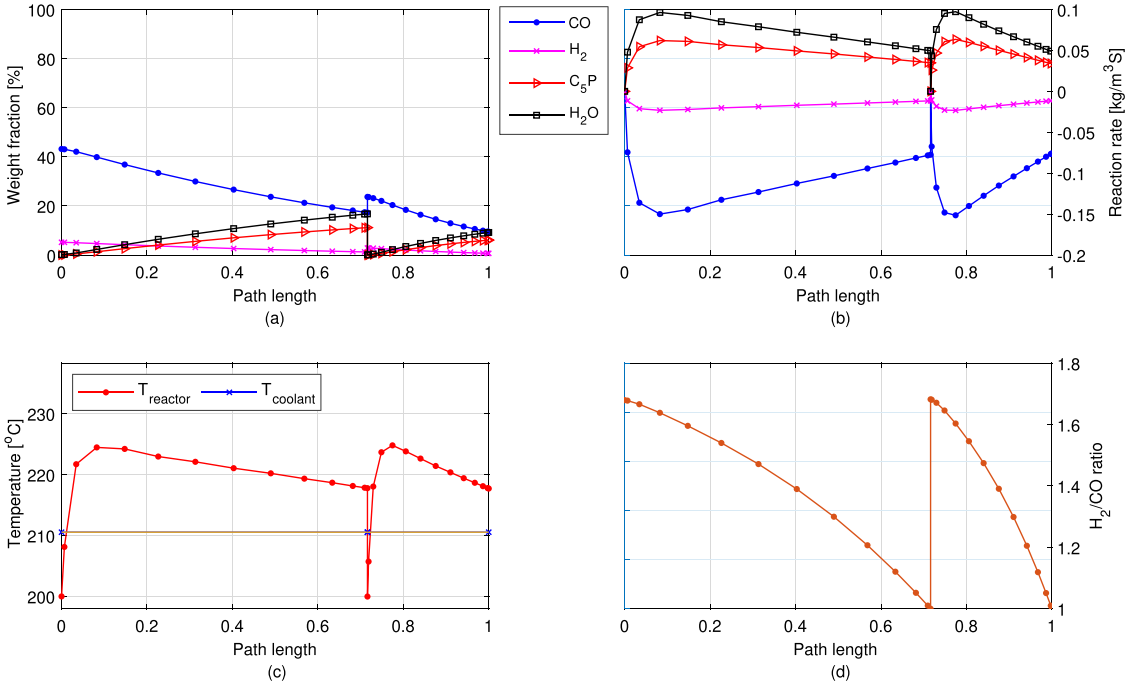

Fig. 5 – (a) Mass concentration, (b) temperature, (c) reaction rate and (d) H_2/CO profile for two-stage optimized design.

Table 6 – Optimized design variables (recycle ratio, volume distribution, catalyst concentration, coolant temperature, makeup H_2 requirement) and production characteristics (net annualized material revenue, C_{5+} production, CO conversion and carbon efficiency) for the single-stage, two-stage and three-stage design with no limitation on CO conversion. The optimized CO-conversion per stage for all cases is 60 % and space time (σ) is set to 5.39 m^3 per kg/s of makeup gas.

Number of stages	Net annualized material revenue [M$/year] per kg/s syngas	Recycle ratio $\frac{W_R}{W_0}$ [–]	Volume distribution $\frac{V_{stage}}{V}$ [%]	Makeup H_2 [–]	C_{5+} production $\frac{W_{C_{5+}}}{W_0}$ [–]	CO conversion X_{CO} [%]	Carbon efficiency $\frac{W_{C,C_{5+}}}{W_{C,0}}$ [%]	Catalyst Conc^n [Kg/m^3]	Coolant T [°C]
1	16.47	2.66	–	0.072	0.263	91.8	77.8	200	210.2
2	17.16	1.44	71.9 % & 28.1 %	0.075	0.274	96.1	81.1	200	210.6
3	17.45	0.55	61.8 %, 25.2 % & 13.0 %	0.075	0.277	97.3	82.1	200	210.2

fraction of CO is much lower for single-stage design due to huge recycling of inert and unreacted syngas in comparison to two-stage design (Fig. 5) and three-stage design (Fig. 2). As a result, the reaction rate is much lower for the single-stage design in comparison to the other two designs. All other profiles look similar to the three-stage once-through design, i.e., the feed H_2/CO ratio at the reactor inlet for all the designs is 1.69 and at the reactor outlet is 1.0 indicating a positive effect of higher selectivity to C_{5+} and lower accrued makeup H_2 cost when the plant is operated at under-stoichiometric and as low H_2/CO as possible. The coolant temperature of approximately 210–211 °C is able to maintain the conversion and production for both single-stage and two-stage optimal design as discussed in the case of once-through three-stage design.

4.2.2. *Comparison of recycled three-stage design against recycled single-stage and two-stage design*

The path optimization is then performed for single-stage, two-stage and three-stage designs with the potential of recycling of tail-gas for all three options without any limit on the maximum total conversion. The results are summarized in Table 6. The results show that it is possible to achieve as high as 96.1 % conversion for two-stage, 4.7 %, higher than the single-stage process and 97.3 % for three-stage process, 5.8 % higher than the single-stage process. In terms of net material value, it is possible to increase the net economic output by 4.2 % and 6 % for two-stage and three-stage designs in comparison to the single-stage design. However, the recycle to makeup gas ratio increases from 0.716 to 1.44 for the two-stage design and from 0 to 0.55 for the three-stage design when there is no restriction on overall CO conversion. The recycle is still much lower than for the single-stage design with the added benefit of an increase in the carbon efficiency of the process by 4.2 %, overall production by 4.2 % when selecting a two-stage design in comparison to the single-stage design. The comparison between two-stage and three-stage is much more unclear as the slight improvement of 1.1 % in production and 1.9 % in objective function comes at the cost of additional stages and design complexity. The three-stage process is also no more once-through and thus requires an additional compressor unit as in the case with the other two designs which makes the two-stage design much more appealing as it can achieve very high CO conversion and syncrude production without added complexity of one more stage. For the optimal volume distribution for two-stage and three-stage design, the number of tubes in each stage is approximately proportional to the material flows to the reactor stages as in the cases discussed in the prior section. The optimal cooling temperature is approximately 210–211 °C and catalyst concentration is 200 kg/m^3. for all three designs suggesting that there is little improvement possibility in these two factors without affecting the total conversion, C_{5+} production and risk of runaway reaction.

The H_2/CO ratio profiles for this case are shown in Fig. 6. The concentration profiles, temperature profiles and reaction rate profiles are similar to Figs. 2, 4 and 5 and is not included here. The H_2/CO profile shows that, with no constraints on the total conversion, it is optimal to operate at slightly higher (still under-stoichiometric) H_2/CO ratio. For the two-stage design, the optimal feed H_2/CO ratio is 1.69 for the first stage and 1.84 for the second stage, while for the three-stage design, the optimal feed H_2/CO ratio is 1.79 for the first stage,

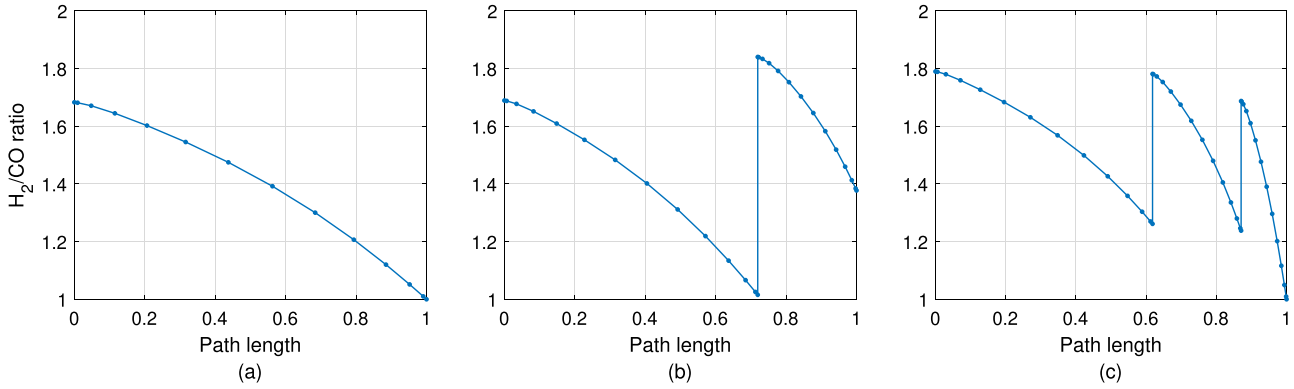

Fig. 6 – H_2/CO profile for optimized single-stage (a), two-stage (b) and three-stage (c) design without any constraints on the total conversion.

1.78 for the second stage and 1.69 for the last stage. The overall flow is higher than the previous case for both two-stage and three-stage designs due to an increase in the recycle ratio for two-stage (increased to 1.44 from 0.716) and three-stage optimized design (increased to 0.55 from 0.0). Thus, H_2/CO is increased to maintain per pass CO conversion to 60 % and achieve as high CO conversion and production of valuable products as possible. The increase in maximum total conversion limit does not have any effect on the single-stage design as it is not possible to increase the total conversion without losing carbon efficiency due to a decrease in C_{5+} selectivity with increased H_2/CO ratio and added cost of extra makeup H_2. Similarly, achieving higher conversion in the case of two-stage and three-stage design by increasing the H_2/CO is not recommended as it comes at the cost of a reduction in carbon efficiency and added makeup H_2 cost.

5. Conclusions

The study presents an optimization of multi-stage FT synthesis using path optimization techniques and suggests an optimized three-stage once through FT design. The optimization strategy is further used to compare an optimized once-through process with single-stage and two-stage design with recycle of tail-gas, and also compares single-stage with two-stage and three-stage designs with recycling. The key conclusion of the studies can be summarized as follows:

- Operating under-stoichiometric H_2/CO feed with maximum possible total CO conversion (93.6 %) and conversion per pass of 60 % is an optimal strategy for once-through three-stage FT synthesis and in general for the FT synthesis over a cobalt catalyst.
- The optimal volume distribution between stages is proportional to the mass flow with 64.4 % and 25.0 % tubes in the first two stages while the coolant temperature is constrained by the maximum allowable peak temperature in the once-through three-stage design.
- With a constraint on the total conversion, the net improvement from switching from a single-stage process to a two-stage and once-through three-stage process is 2.3 % and 2.7 % in terms of syncrude production and 2.8 % and 3.2 % in terms of net material value, while the required recycle to makeup gas ratio is 2.66 and 0.72 for single-stage and two-stage design. Two-stage and once-through three-stage processes perform similarly with less than 1 % difference in total syncrude production, net material costs and carbon efficiency.
- With no constraint on the conversion, two-stage and three-stage processes are 4.2 % and 6 % better than single-stage process in terms of net economic value and 4.2 % and 5.3 % better in terms of syncrude production. The improvement comes at the additional cost of increased material flows (recycle to makeup gas ratio of 1.44 for two-stage and 0.55 for the three stage) and additional complexity of the added stages.

The results discussed here are very much dependent on the catalyst as the peak operating temperature, selectivity to specific products and catalyst degradation in the presence of high water partial pressure are catalyst specific characteristics. The conclusion of similar optimization study using an alternative catalysts could be much different than the one performed in this study. However, for typical cobalt based synthesis, the characteristics are similar to the one used in this study and similar optimization techniques can be employed for a different catalyst. In conclusion, the study recommends the two-stage optimal design to achieve as high CO conversion as possible (96.1 %) with improved production (4.3 % higher than single-stage) and total conversion (4.7 % higher CO conversion than single-stage) without excessive material flows. Although the three-stage process is marginally better in terms of carbon efficiency and syncrude production, the approximate improvement of 1 % comes at the cost of additional stage and design complexity which further reinforces the viability of an optimal two-stage FT design.

Declaration of Competing Interest

The authors have no affiliation with any organization with a direct or indirect financial interest in the subject matter discussed in the manuscript. The following authors have affiliations with organizations with direct or indirect financial interest in the subject matter discussed in the manuscript.

Acknowledgement

The Research Council of Norway (Project no. 280846) is greatly acknowledged for the financial aid of this project.

References

Achenie, L., Biegler, L., 1990. A superstructure based approach to chemical reactor network synthesis. Comput. Chem. Eng. 14 (1), 23–40. https://doi.org/10.1016/0098-1354(90)87003-8. ⟨https://www.sciencedirect.com/science/article/pii/0098135490870038⟩.

Carlsson, L., 2005. From bintulu shell MDS to pearl GTL in Qatar, applying the lessons of eleven years of commericial GTL experience to develop a world scale plant.

Dalai, A., Davis, B., 2008. Fischer-Tropsch synthesis: a review of water effects on the performances of unsupported and supported co catalysts. Appl. Catal. A: Gen. 348 (1), 1–15.

Espinoza, R.L., Zhang, J., Wright, H.A., Harkins, T.H., 2006. Commercial Fischer-Tropsch reactor. United States patents.

Evans, G., Smith, C., 2012. 5.11 – biomass to liquids technology. In: Sayigh, A. (Ed.), Comprehensive Renewable Energy. Elsevier, pp. 155–204. https://doi.org/10.1016/B978-0-08-087872-0.00515-1. (pp).

Feinberg, M., 2002. Toward a theory of process synthesis. Ind. Eng. Chem. Res. 41 (16), 3751–3761. https://doi.org/10.1021/ie010807f

Freund, H., Sundmacher, K., 2008. Towards a methodology for the systematic analysis and design of efficient chemical processes: Part 1. From unit operations to elementary process functions. Chem. Eng. Process.: Process Intensif. 47 (12), 2051–2060. https://doi.org/10.1016/J.CEP.2008.07.011. ⟨https://www.sciencedirect.com/science/article/pii/S0255270108001669⟩.

Gavrilović, L., Jørgensen, E.A., Pandey, U., Putta, K.R., Rout, K.R., Rytter, E., Hillestad, M., Blekkan, E.A., 2021. Fischer-Tropsch synthesis over an alumina-supported cobalt catalyst in a fixed bed reactor-effect of process parameters. Catal. Today 369, 150–157.

Glasser, D., Hildebrandt, D., Crowe, C., 1987. A geometric approach to steady flow reactors: the attainable region and optimization in concentration space. Ind. Eng. Chem. Res. https://doi.org/10.1021/ie00069a014

Hannula, I., 2016. Hydrogen enhancement potential of synthetic biofuels manufacture in the European context: a techno-economic assessment, vol. 104, pp. 199–212. ⟨https://doi.org/10.1016/j.energy.2016.03.119⟩.

Hardeveld, R.M.V., Remans, T.J., Stobbe, E.R., 2013. Stacked catalyst bed for Fischer-Tropsch. United States patents.

Hillestad, M., Ostadi, M., Alamo Serrano, G., Rytter, E., Austbø, B., Pharoah, J., Burheim, O., 2018. Improving carbon efficiency and profitability of the biomass to liquid process with hydrogen from renewable power, vol. 234, pp. 1431–51. ⟨https://doi.org/10.1016/j.fuel.2018.08.004⟩.

Hillestad, M., 2010. Systematic staging in chemical reactor design. Chem. Eng. Sci. 65 (10), 3301–3312. https://doi.org/10.1016/j.ces.2010.02.021

Hillestad, M., 2015. Modeling the Fischer-Tropsch product distribution and model implementation. Chem. Prod. Process Model. 10 (3), 147–159. https://doi.org/10.1515/cppm-2014-0031

Hofbauer, H., Rauch, R., 2019. Biomass to liquid (BtL). Encyclopedia of Sustainability Science and Technology Series, 2nd edition. Springer, New York.

Hydrogen council, 2020. Path to hydrogen competitiveness: a cost perspective.

Jahangiri, H., Bennett, J., Mahjoubi, P., Wilson, K., Gu, S., 2014. A review of advanced catalyst development for Fischer-Tropsch synthesis of hydrocarbons from biomass derived syn-gas. Catal. Sci. Technol. 4, 2210–2229. https://doi.org/10.1039/C4CY00327F

Jiang, Y., Wang, H., Li, S., Yang, C., Zhong, L., Gao, P., Sun, Y., 2020. Toward a full one-pass conversion for the Fischer-Tropsch synthesis over a highly selective cobalt catalyst, vol. 59(no. 17), pp. 8195–201. ⟨https://doi.org/10.1021/acs.iecr.0c00764⟩.

Kolb, T., Eberhard, M., Dahmen, N., Leibold, H., Neuberger, M., Sauer, J., Seifert, H., Zimmerlin, B., 2013. BtL – the bioliq® process at KIT, preprints of the conference.

Larson, E., Williams, R., Kreutz, T., Hannula, I., Lanzini, A., Liu, G., 2012. Energy, environmental, and economic analyses of design concepts for the co-production of fuels and chemicals with electricity via co-gasification of coal and biomass. ⟨https://doi.org/10.2172/1047698⟩, ⟨http://www.osti.gov/servlets/purl/1047698/⟩.

Levenspiel, O., 1962. Chemical Reaction Engineering; An Introduction to the Design of Chemical Reactors. John Wiley and Sons.

Lotfi, R., 2010. Superstructure optimization in heat exchanger network (HEN) synthesis using modular simulators and a genetic algorithm framework. Ind. Eng. Chem. Res. 49 (10), 4731–4737. https://doi.org/10.1021/ie901215w

Martín, M., Grossmann, I.E., 2011. Energy optimization of bioethanol production via gasification of switchgrass. AIChE J. https://doi.org/10.1002/aic.12544

Michailos, S., Bridgwater, A., 2019. A comparative techno-economic assessment of three bio-oil upgrading routes for aviation biofuel production, vol. 43(no. 13), pp. 7206–28, _eprint: ⟨https://doi.org/10.1002/er.4745⟩.

Outi, A., Rautavuoma, I., van der Baan, H.S., 1981. Kinetics and mechanism of the Fischer-Tropsch hydrocarbon synthesis on cobalt on alumina catalyst, vol. 1(no. 5), pp. 247–72, number: 5. ⟨https://doi.org/10.1016/0166-9834(81)80031-0⟩.

Pandey, U., Runningen, A., Gavrilovic, L., Jørgensen, E.A., Putta, K.R., Rout, K.R., Rytter, E., Blekkan, E.A., Hillestad, M., 2021. Modeling Fischer-Tropsch kinetics and product distribution over a cobalt catalyst. AIChE J. 67 (7), e17234. https://doi.org/10.1002/aic.17234

Peschel, A., Freund, H., Sundmacher, K., 2010. Methodology for the design of optimal chemical reactors based on the concept of elementary process functions. Ind. Eng. Chem. Res. 49 (21), 10535–10548. https://doi.org/10.1021/ie100476q

Peschel, A., Karst, F., Freund, H., Sundmacher, K., 2011. Analysis and optimal design of an ethylene oxide reactor. Chem. Eng. Sci. 66 (24), 6453–6469. https://doi.org/10.1016/J.CES.2011.08.054. ⟨https://www.sciencedirect.com/science/article/pii/S0009250911006312?via%3Dihub⟩.

Putta, K.R., Pandey, U., Gavrilovic, L., Rout, K.R., Rytter, E., Blekkan, E.A., Hillestad. M. Optimal renewable energy distribution between gasifier and electrolyzer for syngas generation in a power and biomass-to-liquid fuel process, vol. 9. ⟨https://doi.org/10.3389/fenrg.2021.758149⟩.

Rafiee, A., Hillestad, M., 2012. Staging of the Fischer-Tropsch reactor with an iron based catalyst. Comput. Chem. Eng. 39, 75–83. https://doi.org/10.1016/J.COMPCHEMENG.2011.11.009. ⟨https://www.sciencedirect.com/science/article/pii/S0098135411003309⟩.

Rafiee, A., Hillestad, M., 2013. Staging of the Fischer-Tropsch reactor with a cobalt-based catalyst. Chem. Eng. Technol. 36 (10), 1729–1738. https://doi.org/10.1002/ceat.201200700

Rooney, W.C., Hausberger, B.P., Biegler, L.T., Glasser, D., 2000. Convex attainable region projections for reactor network synthesis. Comput. Chem. Eng. 24 (2–7), 225–229. https://doi.org/10.1016/S0098-1354(00)00518-4. ⟨https://www.sciencedirect.com/science/article/pii/S0098135400005184⟩.

Saeidi, S., Amiri, M.T., Amin, N.A.S., Rahimpour, M.R., 2014. Progress in reactors for high-temperature Fischer-Tropsch process: determination place of intensifier reactor perspective. Int. J. Chem. React. Eng. 12 (1), 639–664. https://doi.org/10.1515/ijcre-2014-0045

Spath, P.L., Dayton, D.C., 2003. Preliminary screening – technical and economic assessment of synthesis gas to fuels and chemicals with emphasis on the potential for biomass-derived syngas, 160.

Storsæter, S., Borg, Ø., Blekkan, E.A., Holmen, A., 2005. Study of the effect of water on Fischer-Tropsch synthesis over supported cobalt catalysts. J. Catal. 231 (2), 405–419.

Swanson, R.M., Platon, A., Satrio, J.A., Brown, R.C. 2010. Techno-economic analysis of biomass-to-liquids production based on gasification, vol. 89, pp. S11–9. ⟨https://doi.org/10.1016/j.fuel.2010.07.027⟩.

Todic, B., Ma, W., Jacobs, G., Davis, B.H., Bukur, D.B., 2014. Co-insertion mechanism based kinetic model of the Fischer-Tropsch synthesis reaction over re-promoted co catalyst. Catal. Today 228, 32–39. https://doi.org/10.1016/J.CATTOD.2013.08.008

Todic, B., Ma, W., Jacobs, G., Davis, B.H., Bukur, D.B., 2015. Corrigendum to: Co-insertion mechanism based kinetic model of the Fischer-Tropsch synthesis reaction over re-promoted co catalyst. Catal. Today 242, 386. https://doi.org/10.1016/J.CATTOD.2014.08.020. ⟨https://www.sciencedirect.com/science/article/pii/S0920586114005999⟩.

Tucker, C.L., van Steen, E., 2020. Activity and selectivity of a cobalt-based Fischer-Tropsch catalyst operating at high conversion for once-through biomass-to-liquid operation, vol. 342, pp. 115–23. ⟨https://doi.org/10.1016/j.cattod.2018.12.049⟩, ⟨https://www.sciencedirect.com/science/article/pii/S0920586118306862⟩.

Tucker, C.L., Bordoloi, A., Steen, E.v., 2021. Novel single pass biogas-to-diesel process using a Fischer-Tropsch catalyst designed for high conversion, vol. 5(no. 22), pp. 5717–32. ⟨https://doi.org/10.1039/D1SE01299A⟩, ⟨https://pubs.rsc.org/en/content/articlelanding/2021/se/d1se01299a⟩.

Ugray, Z., Lasdon, L., Plummer, J., Glover, F., Kelly, J., Martí, R., 2007. Scatter search and local nlp solvers: a multistart framework for global optimization. INFORMS J. Comput. 19 (3), 328–340.

Yeomans, H., Grossmann, I.E., 1999. A systematic modeling framework of superstructure optimization in process synthesis. Comput. Chem. Eng. 23 (6), 709–731. https://doi.org/10.1016/S0098-1354(99)00003-4. ⟨https://www.sciencedirect.com/science/article/pii/S0098135499000034⟩.